Andrographolide sodium bisulfate attenuates UV-induced photo-damage by activating the keap1/Nrf2 pathway and downregulating the NF-κB pathway in HaCaT keratinocytes

MEI-LING WANG[1*], QING-YUAN ZHONG[2*], BAO-QIN LIN[2], YU-HONG LIU[1], YAN-FENG HUANG[1], YANG CHEN[2], JIE YUAN[1], ZI-REN SU[1] and JANIS YA-XIAN ZHAN[2]

[1]Mathematical Engineering Academy of Chinese Medicine, [2]School of Pharmaceutical Sciences, Guangzhou University of Chinese Medicine, Guangzhou, Guangdong 510006, P.R. China

Received April 28, 2019; Accepted October 9, 2019

DOI: 10.3892/ijmm.2019.4415

Abstract. Oxidative and inflammatory damage has been suggested to play important roles in the pathogenesis of skin photoaging. Andrographolide sodium bisulfate (ASB) is a soluble derivative of andrographolide and has known antioxidant and anti-inflammatory properties. In the present study, cellular experiments were designed to investigate the molecular mechanisms underlying the effect of ASB in relieving ultraviolet (UV)-induced photo-damage. Following ASB pretreatment and UV irradiation, the apoptosis and necrosis of HaCaT cells were investigated by Hoechst 33342/propidium iodide staining. Reactive oxygen species (ROS) production was investigated using a DCFH-DA fluorescence probe. Furthermore, the protein expression levels of p65, NF-κB inhibitor-α, nuclear factor E2-related factor 2 (Nrf2) and kelch-like ECH-associated protein 1 (keap1) were measured via western blotting and immunofluorescence analyses. Furthermore, NF-κB-mediated cytokines were assessed by ELISA, and Nrf2-mediated genes were detected by reverse transcription-quantitative PCR. Pretreatment with ASB markedly increased cell viability, decreased cell apoptosis and decreased UV-induced excess ROS levels. In addition, ASB activated the production of Nrf2 and increased the mRNA expression levels of glutamate-cysteine ligase catalytic subunit and NAD(P)H quinone oxidoreductase 1, while ASB downregulated the protein expression of p65 and decreased the production of interleukin (IL)-1β, IL-6 and tumor necrosis factor-α. These results suggested that ASB attenuates UV-induced photo-damage by activating the keap1/Nrf2 pathway and downregulating the NF-κB pathway in HaCaT keratinocytes.

Correspondence to: Professor Zi-Ren Su, Mathematical Engineering Academy of Chinese Medicine, Guangzhou University of Chinese Medicine, 223 Waihuan Road, Guangzhou, Guangdong 510006, P.R. China
E-mail: suziren@gzucm.edu

Professor Janis Ya-Xian Zhan, School of Pharmaceutical Sciences, Guangzhou University of Chinese Medicine, 223 Waihuan Road, Guangzhou, Guangdong 510006, P.R. China
E-mail: zyx@gzucm.edu.cn

*Contributed equally

Key words: andrographolide sodium bisulfate, nuclear factor E2-related factor 2, NF-κB, ultraviolet, photo-damage

Introduction

Skin photodamage is a specific type of damage to skin tissue produced by ultraviolet (UV) irradiation. It is characterized by erythema, edema, dyspigmentation, sallowness, fine and coarse wrinkles, telangiectasia and roughness (1,2). A number of studies have demonstrated that ~80% of exposed skin aging is caused by UV-induced photo-damage (3,4). The risk of skin aging in high-exposure populations is twice as high as that in low-exposure populations, and the onset time of aging could be 10 years earlier (5).

UV-induced oxidative stress and inflammatory damage are considered to play important roles in the occurrence of photodamage (6,7). The NF-κB signaling pathway, activated by UV-induced reactive oxygen species (ROS), is an important cell signaling pathway in the process of skin inflammation and aging (8,9). NF-κB exists in an inactive state in the cytoplasm due to NF-κB inhibitors under non-inflammatory conditions. The activation of the NF-κB is initiated by inhibitor of NF-κB (IκB) kinase (IKK), which degrades cytoplasmic IκB protein, thereby triggering the rapid release of NF-κB from IκB and intranuclear translocation (10). UV-induced excess ROS activate IKK, which phosphorylates IκBα and activates NF-κB (11). Activated NF-κB subsequently translocates from the cytosol to the nucleus, where it promotes the release of various proinflammatory cytokines and chemokines, including tumor necrosis factor-α (TNF-α), interleukin-6 (IL-6) and interleukin-1β (IL-1β) (12). It also upregulates key matrix metalloproteinases (MMPs) and degrades extracellular matrix components, thus leading to photoaging (13).

In addition, under oxidizing conditions, the increased ROS also activate the nuclear factor E2-related factor 2 (Nrf2)

signaling pathway (8). Activation of the Nrf2 signaling pathway plays a pivotal role in maintaining the cellular redox balance and protecting against inflammation by activating antioxidant cascades (14). On the one hand, moderate levels of ROS from solar radiation induce Nrf2 activation; when cells are activated by ROS or some other nucleophilic agent, Nrf2 uncouples from kelch-like ECH-associated protein 1 (keap1) (15). The activated Nrf2 is translocated into the nucleus, then combines with antioxidant response element (ARE), which results in a cytoprotective adaptive response (16). The primary target genes of Nrf2 include glutamate-cysteine ligase catalytic subunit (GCLC), hemeoxygenase-1 and NAD(P)H quinone oxidoreductase 1 (NQO1) (17). These antioxidant genes help to eliminate excessive ROS to decrease oxidative stress and the inflammatory response (18). On the other hand, excessive ROS induced by high-dose UV inactivate Nrf2 and block the Nrf2/ARE signal transduction pathway, which results in decreased activity of antioxidant enzymes and a disturbed antioxidant defense system; therefore, the damage is exacerbated (19).

Andrographolide sodium bisulfate (ASB), a soluble derivative composed of andrographolide and sodium bisulfate, has excellent water solubility (20). Intravenous infusion of ASB at 150 mg/kg body weight is considered safe for rats (21). ASB has anti-inflammatory, antipyretic and analgesic activities (22). ASB is associated with blockage of oxidative damage and NF-κB-mediated inflammation in diabetic cardiomyopathy (23), and ASB has advantages over andrographolide for the treatment of LPS-induced lesions (20). A previous study demonstrated that ASB prevents UV-induced skin photodamage by inhibiting oxidative stress and inflammation *in vivo* (24); however, the associated underlying mechanisms remain unclear. The aim of the present study was to investigate the effects and underlying mechanisms of action of ASB on oxidative stress and inflammation in UV-induced photodamage in HaCaT cells.

Materials and methods

Chemicals and reagents. ASB (cat. no. 111655-201503; purity >98%) was purchased from the National Institutes for Food and Drug Control (Fig. S1). Anti-Nrf2 rabbit antibody (cat. no. ab62352), anti-keap1 rabbit antibody (cat. no. ab218815), anti-IκBα rabbit antibody (cat. no. ab32518) and anti-Lamin B1 rabbit antibody (cat. no. ab16048) were purchased from Abcam. Anti-p65 rabbit antibody (cat. no. 8242S) and anti-GAPDH rabbit antibody (cat. no. 14C10) were purchased from Cell Signaling Technology, Inc. Goat anti-rabbit lgG H&L [horseradish peroxidase (HRP)] (cat. no. ab6721) was purchased from Abcam. DyLight 488-conjugated goat anti-rabbit lgG H&L was purchased from Abbkine Scientific Co., Ltd. (cat. no. A23220). DMEM, FBS and penicillin/streptomycin were purchased from Gibco; Thermo Fisher Scientific, Inc. PBS was bought from HyClone; GE Healthcare Life Sciences. MTT was purchased from BioFrox (cat. no. 3580MG250; http://www.saiguobio.com/info.aspx?id=230).

Cell culture. HaCaT cells were donated by the Guangdong Hospital of Traditional Chinese Medicine (Guangzhou, China). Cells were cultured in DMEM containing 10% FBS and 1% (v/v) antibodies (50 U/ml penicillin and 50 mg/ml streptomycin) in an atmosphere of 5% CO_2 at 37˚C.

UV irradiation. Cells were pretreated with ASB (10, 30 and 100 μM) or DMEM for 24 h. The cells were then washed with PBS twice and covered with a thin layer of PBS to avoid drying. The cells were subsequently exposed to 300 μW/cm^2•sec UV for 300 sec (a total dose of 90 mJ/cm^2) with a UVB 3.0 halogen lamp (UVA, 320-400 nm; UVB, 275-320 nm; UVA/UVB =97:3; NPMOYPET®). Following UV irradiation, cells were re-covered with fresh DMEM.

MTT assay. HaCaT cells (3.5x10^4/ml) were plated in 96-well plates, and then treated with different concentrations of ASB (0, 0.01, 0.1, 1, 10, 100, 500, 1,000 or 2,000 μM) for 24 h. An MTT assay was used to measure the cytotoxicity of ASB. In addition, in order to study the effect of ASB on UV-induced HaCaT cells, cells were pretreated with ASB (10, 30 and 100 μM) for 24 h. After UV irradiation (300 μW/cm^2 sec x 300 sec), cells were re-covered with fresh medium and cultured for 24 h. The MTT assay was then performed. HaCaT cells were stained with MTT (5 mg/ml) at 37˚C for 4 h. The medium was removed, and 150 μl DMSO was then added to each well. The optical density was measured at 490 nm. The absorbance of the control cells was considered equal to the viability.

Assessment of morphological changes using fluorescence microscopy. Apoptotic and necrotic cells were determined with Hoechst 33342 and propidium iodide (PI) double staining as previously described (25). In brief, HaCaT cells (3.5x10^4/ml) were pretreated with ASB at concentrations of 10, 30 and 100 μM for 24 h and then irradiated by UV (300 μW/cm^2 sec x 300 sec). Cells were re-covered with fresh medium and cultured for 12 h. Cells were then incubated with 1 ml Hoechst 33342 solution (10 μg/ml) for 25 min and incubated with 1 ml PI (2.5 μg/ml) in the dark for 15 min. After staining, the fluorescence intensity was observed under a fluorescence microscope (original magnification, x100; BX53; Olympus Corporation), and the fluorescence was measured at 400-500 nm emission for Hoechst 33342 dye, and >630 nm emission for PI.

Measurement of intracellular production of ROS. Intracellular ROS levels were determined by the oxidative conversion of cell-permeable 2',7'-dichlorodihydro-fluorescein diacetate (DCFH-DA) to fluorescent DCF, as previously described (26). Cells (3.5x10^4/ml) were seeded in a 96-well plate and pretreated with DMEM containing ASB for 24 h. Then, the cells were irradiated with UV (300 μW/cm^2 sec x 300 sec). The cells were then cultured with fresh medium for 1 h. Subsequently, the cells were washed twice with PBS and incubated with 1 ml DCFH-DA (6 μM) solution for 30 min at 37˚C. The cells were further washed twice with PBS, and DCFH-DA fluorescence was measured using a fluorescence microscope connected to an imaging system (original magnification, x200; BX53; Olympus Corporation). The fluorescence was measured at 525 nm emission for DCFH-DA, and the fluorescence intensity over the entire field of vision was measured using Image J software (version 1.48; National Institutes of Health).

Measurement of inflammatory cytokines. HaCaT cells ($3.5x10^4$/ml) were pretreated with different concentrations of ASB for 24 h and then irradiated with UV (300 μW/cm^2 sec x 300 sec). Cells were re-covered with fresh DMEM medium and cultured for 12 h. Subsequently, the supernatant was collected for further experiments. Levels of TNF-α (cat. no. CSB-E04740h), IL-6 (cat. no. CSB-E04638h) and IL-1β (cat. no. CSB-E08053h) in the supernatant of HaCaT cells were detected using commercially available ELISA kits (Cusabio Technology LLC), according to the manufacturer's protocol.

Immunofluorescence staining. The nuclear translocation of Nrf2 and p65 was measured via immunofluorescence. HaCaT cells ($3.5x10^4$/ml) grown in laser confocal petri dishes were incubated with ASB for 24 h. The cells were then irradiated with UV (300 μW/cm^2 sec x 300 sec). Following UV irradiation, the cells were washed three times with PBS (3 min each), fixed with 4% paraformaldehyde for 15 min at room temperature, permeabilized with Triton X (0.5% in PBS) for 20 min, then washed and blocked with 5% goat serum (Beijing Solarbio Science & Technology Co., Ltd.) for 30 min at room temperature. The cells were then stained with primary antibodies (Nrf2, 1:100; Nrf2, 1:400) at 4˚C overnight, washed with PBS with Tween-20 (PBST; 0.5% Tween-20 in PBS) and incubated with fluorochrome-conjugated secondary antibodies (1:200) for 1 h at room temperature. The cells were then incubated for 5 min with DAPI (5 μg/ml) in the dark, washed with PBST four times and mounted on microscopic slides with a drop of fluorescent mounting medium at room temperature. The antibody localization was visualized using a fluorescence microscope (original magnification, x200; BX53; Olympus Corporation).

Reverse transcription-quantitative PCR (RT-qPCR). HaCaT cells ($3.5x10^4$/ml) were solubilized with TRIzol® reagent (Invitrogen; Thermo Fisher Scientific, Inc.). Total RNA was extracted according to the manufacturer's protocol. First-strand cDNA was synthesized from 500 ng total RNA using Bestar™ Moloney Murine Leukemia Virus reverse transcriptase (DBI® Bioscience). The reaction conditions were 37˚C for 15 min, 98˚C for 5 min, and holding at 4˚C. Then, the cDNA was amplified for individual PCR reactions using Bestar™ SybrGreen qPCR Mastermix (DBI® Bioscience). The primer sequences used were as follows: GCLC sense, 5'-CTGGAG CAACCTACTGTCTAA-3' and antisense, 5'-TCAGGTCCC AGGTAGTCTTTA-3'; NQO1 sense, 5'-TCTCCTCATCCT GTACCTCTTT-3' and antisense, 5'-CTGGAGCAACCTACT GTCTAAG-3'; and GAPDH sense, 5'-GGAGTCAACGGA TTTGGTCGT-3' and antisense, 5'-GCTTCCCGTTCTCAG CCTTGA-3'. The reaction conditions were as follows: Initial denaturation at 95˚C for 2 min; DNA amplification at 95˚C for 10 sec, 55˚C for 30 sec and 72˚C for 30 sec (40 cycles); and a final extension step of 65-95˚C (5 sec/cycle; 0.5˚C/cycle) for 38 cycles. The level of mRNA was normalized to the level of GAPDH, and compared with the normal control (NC) group (treated with the same volume of complete DMEM) using the $2^{-\Delta\Delta Cq}$ method (27).

Western blot analysis. Proteins expression was measured by western blotting as described previously (28). Nuclear and cytoplasmic proteins were extracted from cultured cells using a nuclear or cytoplasmic protein extraction kit (Beyotime Institute of Biotechnology), respectively (Cells were seeded into plates at a density of 3.5 x 10^4/ml). Protein concentrations were measured using a BCA protein assay kit (Beyotime Institute of Biotechnology). Then, cell lysates (10 μg/lane) were separated by SDS-PAGE (10%) and electrophoretically transferred onto a polyvinylidene fluoride membrane. The membrane was then washed with TBS with Tween-20 (TBST) three times, and blocked with 5% non-fat milk in TBST (1% Tween-20) for 2 h at room temperature. The membrane was incubated with Nrf2 (1:1,000), keap1 (1:300), p65 (1:3,000), IκBα (1:1,000), GAPDH (1:1,000) and Lamin B (1:1,000) antibodies overnight at 4˚C, and incubated with HRP-coupled secondary antibodies (1:2,000) for 1 h at room temperature. Proteins were detected using enhanced chemiluminescence (Fdbio Science). The protein intensity was measured using Image J software (version 1.48; National Institutes of Health). The relative protein levels were normalized to GAPDH/Lamin B1 protein.

Statistical analysis. All data are expressed as the mean ± SD. Statistical analyses were performed using SPSS 20 (IBM Corp.). Group differences were assessed by one-way ANOVA followed by Tukey's test for multiple comparisons. $P<0.05$ was considered to indicate a statistically significant difference.

Results

ASB increases the cell viability of UV-induced HaCaT cells. As presented in Fig. 1A, 0.01-2,000 μM ASB exerted no cytotoxic effect on HaCaT cells. Compared with the NC group, the viability of UV-induced HaCaT cells was significantly decreased ($P<0.01$). However, the decreased cell viability was significantly increased by ASB, and ASB at a concentration of 100 μM increased cell viability by nearly 1-fold ($P<0.01$ vs. UV-alone group; Fig. 1B).

ASB inhibits the UV-induced apoptosis and necrosis of HaCaT cells. As presented in Fig. 1C, under observation with ordinary light following UV irradiation, the number of the HaCaT cells was decreased and the cell refraction and adhesion abilities were weakened. ASB treatment markedly increased cell number, restored cell morphology, and enhanced cell refraction and adhesion abilities. Furthermore, the observation with fluorescent light detected that, compared with the NC group, the number of apoptotic cells (bright blue) in the UV group was increased, which manifested as decreased cell volume and nuclear fragmentation. At the same time, a number of necrotic cells (bright red) appeared. However, compared with the UV group, preincubation with ASB decreased the number of apoptotic and necrotic cells.

ASB inhibits oxidative stress in UV-induced HaCaT cells. In order to investigate whether ASB could decrease the UV-induced oxidative stress, the ROS production was investigated using the fluorescent ROS probe DCFH-DA, and the mRNA expression levels of antioxidant genes were measured by RT-qPCR. As presented in Fig. 2A, UV irradiation (90 mJ/cm^2) increased the production of ROS, which was significantly higher than that in the NC group ($P<0.01$; Fig. 2A and B). Furthermore, the mRNA

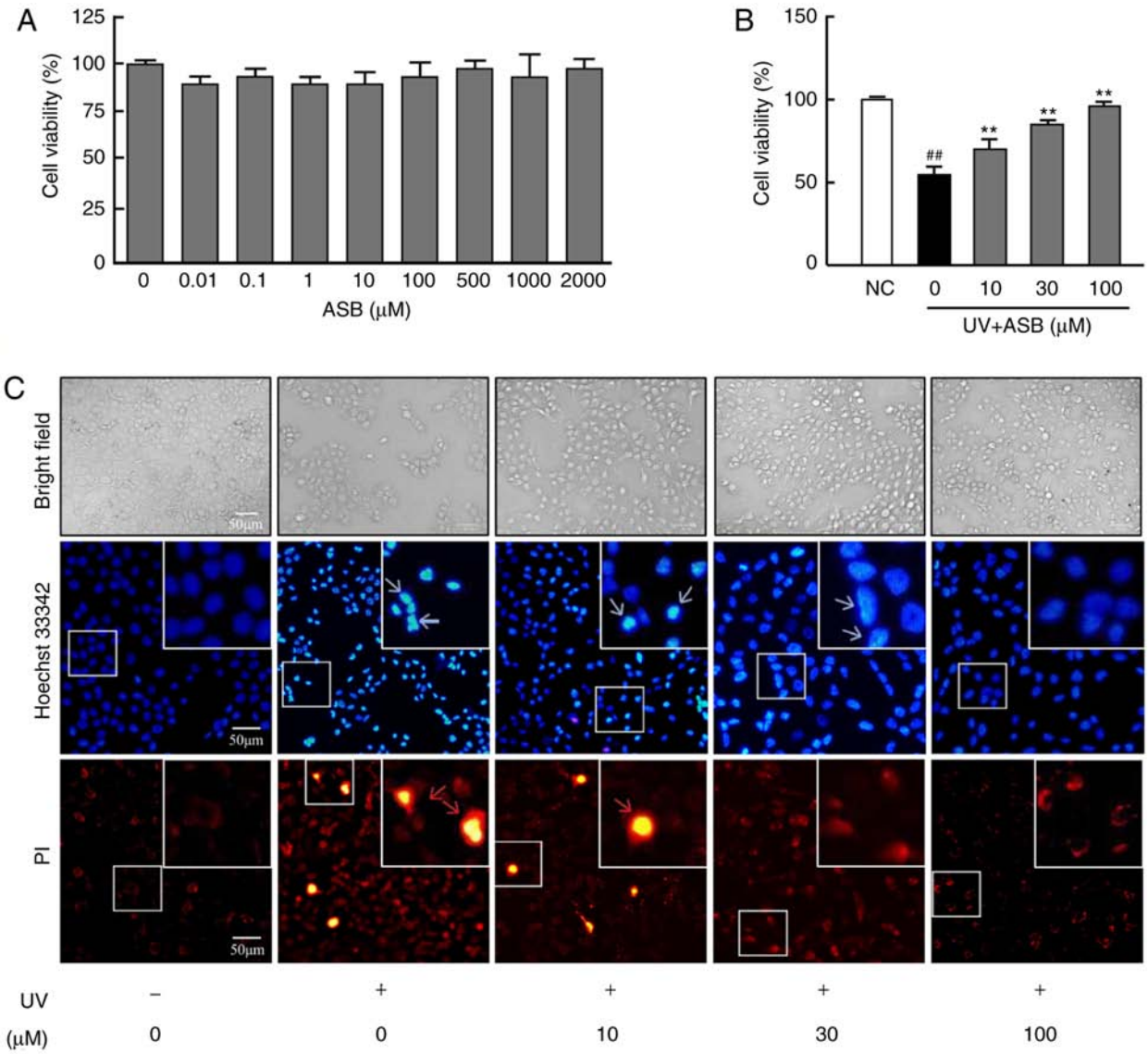

Figure 1. Protective effect of ASB on UV-induced HaCaT cells. (A) The cells were treated with 0, 0.01, 0.1, 1, 10, 100, 500, 1,000 and 2,000 μM ASB for 24 h. The cell viability was determined by MTT assay (n=5 for each group). (B) The cells were preincubated with ASB (10, 30 and 100 μM) and irradiated with UV (90 mJ/cm^2). Cell viability was measured by MTT assay (n=5 for each group). (C) The cells were preincubated with ASB (10, 30 and 100 μM) and irradiated with UV (90 mJ/cm^2). Cell apoptosis and death were measured by staining with Hoechst 33342 and PI. The blue arrowheads indicate apoptotic cells, and the red arrowheads indicate dead cells. The images were examined by bright field and fluorescence microscopy. The results are expressed as the mean ± SD. $^{\#\#}$P<0.01 vs. NC group; **P<0.01 vs. UV-alone group. UV, ultraviolet; ASB, andrographolide sodium bisulfite; NC, normal control; PI, propidium iodide.

expression levels of GCLC and NQO1 in the UV group were lower than those in the NC group (P<0.05; Fig. 2C and D). Notably, ASB pretreatment inhibited the UV-induced ROS production (P<0.01; Fig. 2A and B), and high concentrations of ASB significantly upregulated GCLC and NQO1 expression levels by nearly 1-fold and 1.6-fold respectively (P<0.05 vs. UV group; Fig. 2C and D).

ASB alleviates inflammatory cytokine production in UV-induced HaCaT cells. The results revealed that UV-induced HaCaT cells exhibited excessive production of IL-1β, IL-6 and TNF-α. Conversely, ASB pretreatment efficiently decreased the UV-induced expression of IL-1β, IL-6 and TNF-α. ASB at 100 μM decreased IL-1β, IL-6 and TNF-α levels by nearly 2-fold, 3-fold and 1.5-fold, respectively (P<0.01 vs. UV group; Fig. 2E-G).

Effect of UV irradiation on the NF-κB and Nrf2 signaling pathways. As presented in Fig. 3, UV induced the abnormal expression of p65, IκBα, Nrf2 and keap1 in the cytosol and nucleus in a time-dependent manner. Following UV irradiation, the protein expression levels of p65 and IκBα in the cytosol increased between 0 and 6 h, while the nuclear expression of p65 increased from 0.5 h, peaked at 2 h, and then gradually decreased thereafter (Fig. 3). By contrast, the protein expression levels of Nrf2 in the cytosol and nucleus and keap1 started to rise between 0 and 3 h, peaked around 3 h, and then gradually decreased (Fig. 3).

ASB activates the Nrf2 signaling pathway in UV-induced HaCaT cells. As presented in Fig. 4, the expression levels of keap1 and nuclear Nrf2 were significantly down-regulated in the UV-induced group (P<0.05 vs. NC group;

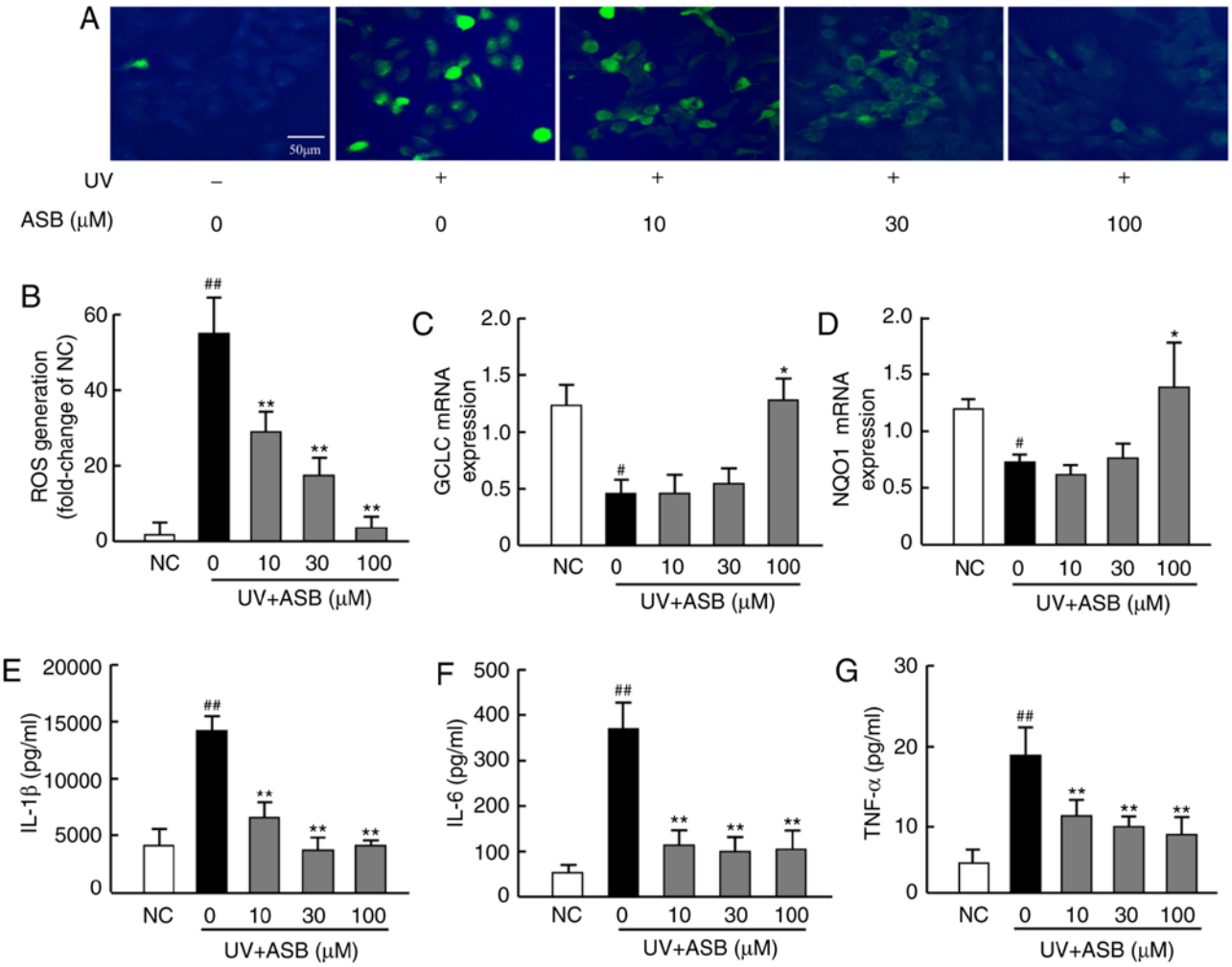

Figure 2. ASB decreases oxidative stress and proinflammatory cytokines in UV-irradiated HaCaT cells. The cells were preincubated with ASB (10, 30 and 100 μM) and irradiated with UV (90 mJ/cm^2). (A) The intracellular ROS in HaCaT cells was assessed by DCFH-DA. The appearance of green fluorescence represents the intensity of the generated ROS. (B) The fluorescence intensity was quantified with Image J software. The mRNA expression levels of (C) GCLC and (D) NQO1 in HaCaT cells were measured by reverse transcription-quantitative PCR. The production of (E) IL-1β, (F) IL-6 and (G) TNF-α was measured by ELISA (n=4 for each group). The results are expressed as the mean ± SD. $^{\#}$P<0.05, $^{\#\#}$P<0.01 vs. NC group; *P<0.05, **P<0.01 vs. UV-alone group. UV, ultraviolet; ASB, andrographolide sodium bisulfite; ROS, reactive oxygen species; GCLC, glutamate-cysteine ligase catalytic subunit; NQO1, NAD(P)H quinone oxidoreductase 1; IL-1β, interleukin-1β; IL-6, interleukin-6; TNF-α, tumor necrosis factor-α; NC, normal control.

Fig. 4A, B and D). Conversely, ASB pretreatment increased the protein expression levels of keap1, cytoplasmic and nuclear Nrf2 in a dose-dependent manner (P<0.05 or P<0.01 vs. UV group; Fig. 4). Furthermore, ASB at a high concentration was able to increase the expression levels of keap1, cytoplasmic Nrf2 and nuclear Nrf2 by nearly 1.9-fold, 1.9-fold and 2.1-fold respectively. Notably, the fluorescence intensity of Nrf2 was in accordance with the western blotting results. The immunofluorescence staining results indicated that the fluorescence intensity of Nrf2 in the nucleus was decreased in UV-induced cells. However, ASB pretreatment markedly reversed the abnormal nuclear translocation of Nrf2 (Fig. 5).

ASB inhibits the NF-κB signaling pathway in UV-induced HaCaT cells. As presented in Fig. 6, the expression levels of IκBα, cytoplasmic p65 and nuclear p65 were significantly upregulated in the UV-induced group (P<0.05 or P<0.01 vs. NC group). The moderate concentration of ASB significantly decreased the protein expression level of p65 in the nucleus, while high concentrations were able to downregulate the expression levels of IκBα, cytoplasmic p65 and nuclear p65 by 61.7, 52.6 and 46.4%, respectively (P<0.05 or P<0.01 vs. UV group; Fig. 6B-D). In particular, the fluorescence intensity of p65 was in accordance with the western blotting results. The immunofluorescence staining results indicated that the fluorescence intensity of p65 in the nucleus was increased in UV-induced cells. However, ASB pretreatment markedly reversed the abnormal nuclear translocation of p65 (Fig. 7).

Discussion

UV irradiation is a predominant environmental factor in the pathogenesis of photo-damage. Over time it is possible to develop actinic keratosis and skin cancer (29). It has been reported that the oxidative stress and inflammatory response mediated by UV are critical factors in the pathogenesis of photo-aging (6,7). Thus the development of effective anti-UV-induced photoaging drugs will focus on the prevention of oxidative damage and inflammation during photoaging. ASB has potential antioxidant and anti-inflammatory activities, and a

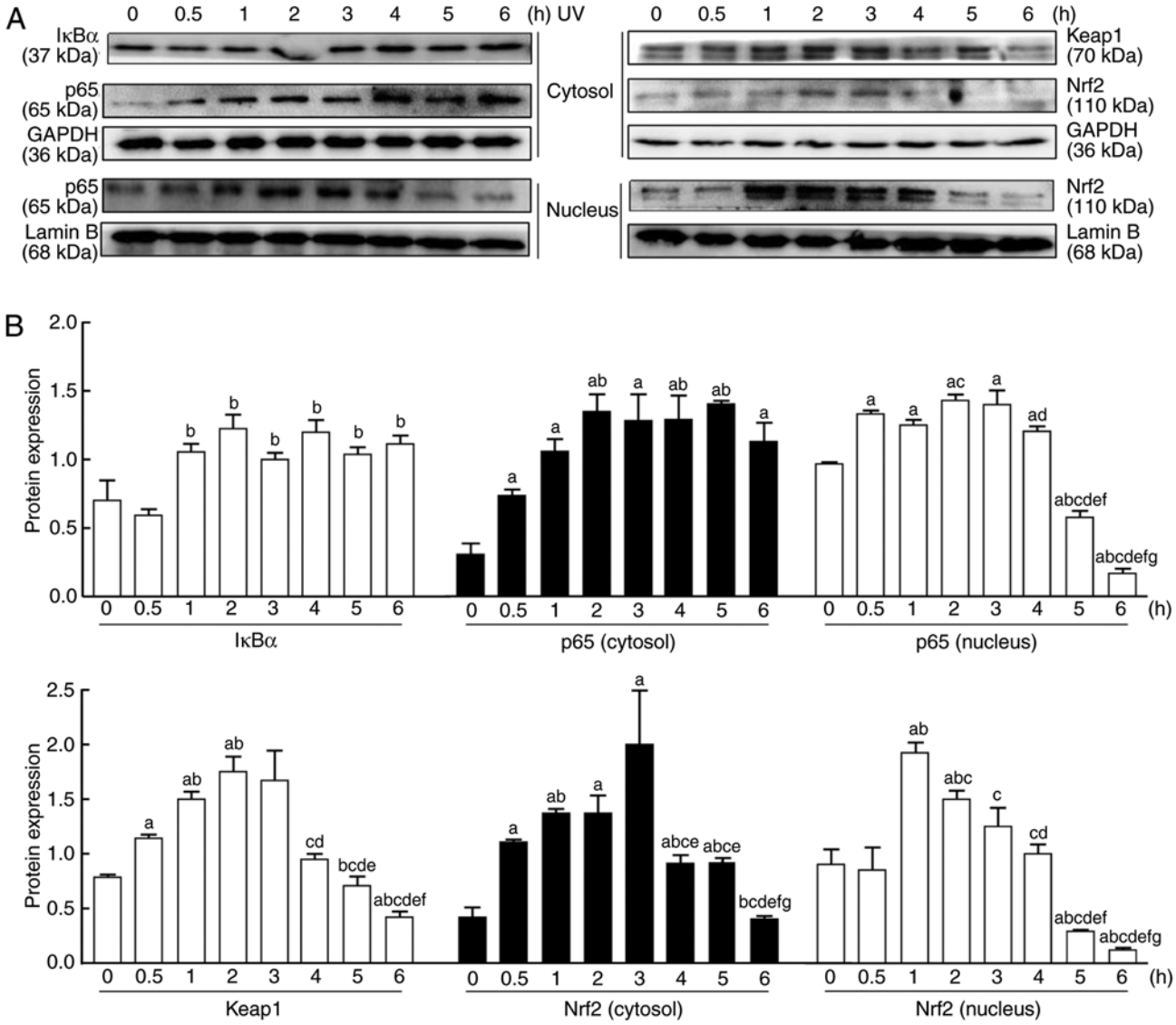

Figure 3. Changes in the Nrf2 and NF-κB signaling pathways in HaCaT cells after UV irradiation. (A) Nuclear and cytoplasmic proteins were extracted from the cultured cells at 0, 0.5, 1, 2, 3, 4, 5 and 6 h after UV irradiation (90 mJ/cm^2). The protein expression levels of NF-κB-mediated p65, and IκBα and Nrf2-mediated Nrf2 and keap1, were measured by western blotting. (B) Relative changes in protein intensities were quantified by densitometric analysis and are presented as bar diagrams (n=3 for each group). The results are expressed as the mean ± SD. [a]P<0.05 vs. the 0 h group; [b]P<0.05 vs. the 0.5 h group; [c]P<0.05 vs. the 1 h group; [d]P<0.05 vs. the 2 h group; [e]P<0.05 vs. the 3 h group; [f]P<0.05 vs. the 4 h group; [g]P<0.05 vs. the 5 h group. UV, ultraviolet; IκBα, NF-κB inhibitor-α; keap1, kelch-like ECH-associated protein 1; Nrf2, nuclear factor E2-related factor 2.

previous study reported that ASB could prevent UV-induced skin photo-damage *in vivo* (24).

Excessive UV exposure could accelerate the accumulation of ROS in the skin, increasing oxidative stress in cutaneous cells, thereby resulting in photodamage. UV-induced ROS production activates the NF-κB signaling pathway, which further induces inflammation and apoptosis in cells and causes skin aging (8,30). In its inactive form, NF-κB is sequestered in the cytoplasm and bound by members of the IκB family of inhibitor proteins. Accumulation of ROS that activate NF-κB causes the nuclear localization of p65 (8). In the nucleus, NF-κB binds to a consensus sequence (5'GGGACTTTCC-3') in various genes (such as IL-1β, IL-6 and TNF-α), and thus activates their transcription. Furthermore, proinflammatory cytokines subsequently stimulate the signal transduction pathway to activate NF-κB, thus causing a feedback loop (12). Such inflammatory mediators further promote the expression levels of MMPs (13). The results of the present study demonstrated that UV irradiation could cause HaCaT cell apoptosis via qualitative analysis, which will be confirmed through quantitative analysis in a further study. The results also showed that UV irradiation could upregulate ROS, p65 and IκBα levels, as well as the production of IL-1β, IL-6 and TNF-α cytokines in HaCaT cells. However, ASB pretreatment significantly decreased the UV-induced accumulation of ROS, and downregulated the protein expression of p65 in the nucleus, while subsequently lessening the secretion of proinflammatory cytokines and reducing the apoptosis of HaCaT cells.

The Nrf2 pathway is an important antioxidative and anti-inflammatory pathway involved in UV-ROS-induced skin damage (31). Under normal physiological conditions, keap1 is associated with Nrf2. However, under oxidizing conditions, the increased level of ROS promotes the dissociation of Nrf2 and keap1, and dissociated Nrf2 translocates to the nucleus, combines

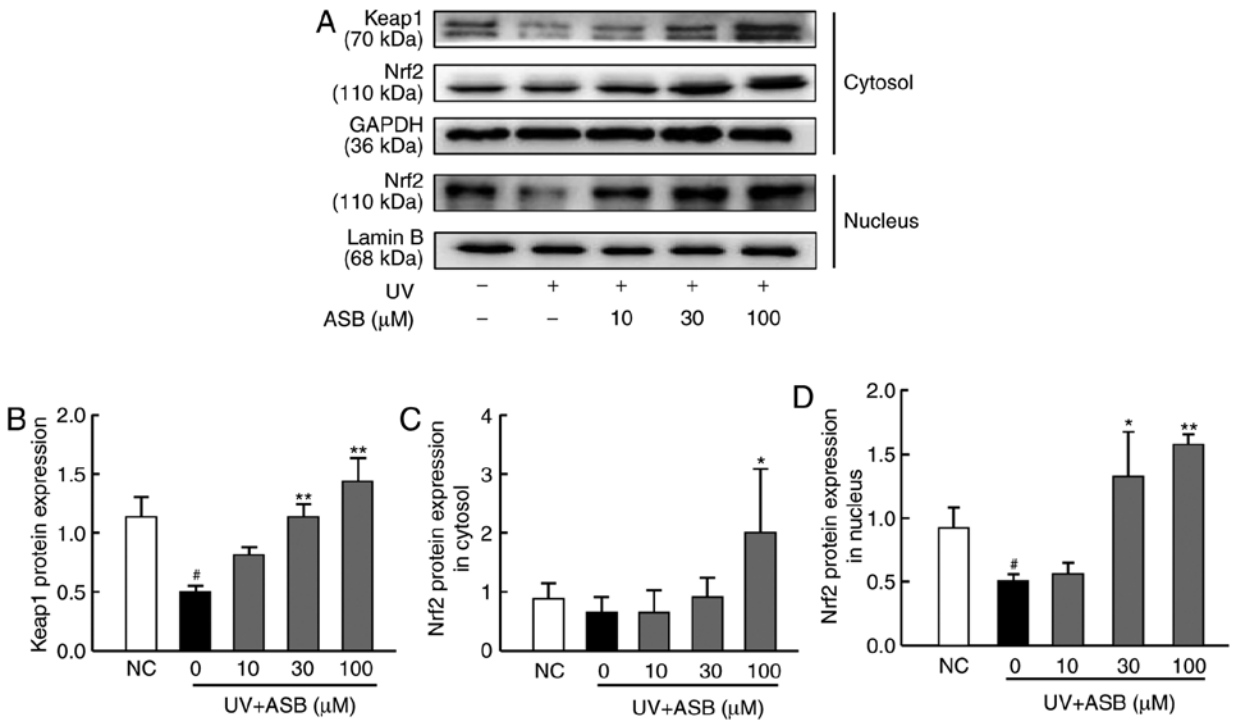

Figure 4. ASB activates the Nrf2 signaling pathway in UV-induced HaCaT cells. The cells were preincubated with ASB (10, 30 and 100 μM) and irradiated with UV (90 mJ/cm^2). (A) Nuclear and cytoplasmic proteins were extracted; Nrf2 and keap1 proteins were measured by western blotting. Relative changes in protein intensity were quantified for (B) keap1, (C) cytosolic Nrf2 and (D) nuclear Nrf2 by densitometric analysis, and are presented as bar diagrams (n=3 for each group). $^{\#}$P<0.05 vs. NC group; *P<0.05, **P<0.01 vs. UV-alone group. ASB, andrographolide sodium bisulfite; UV, ultraviolet; keap1, kelch-like ECH-associated protein 1; Nrf2, nuclear factor E2-related factor 2; NC, normal control.

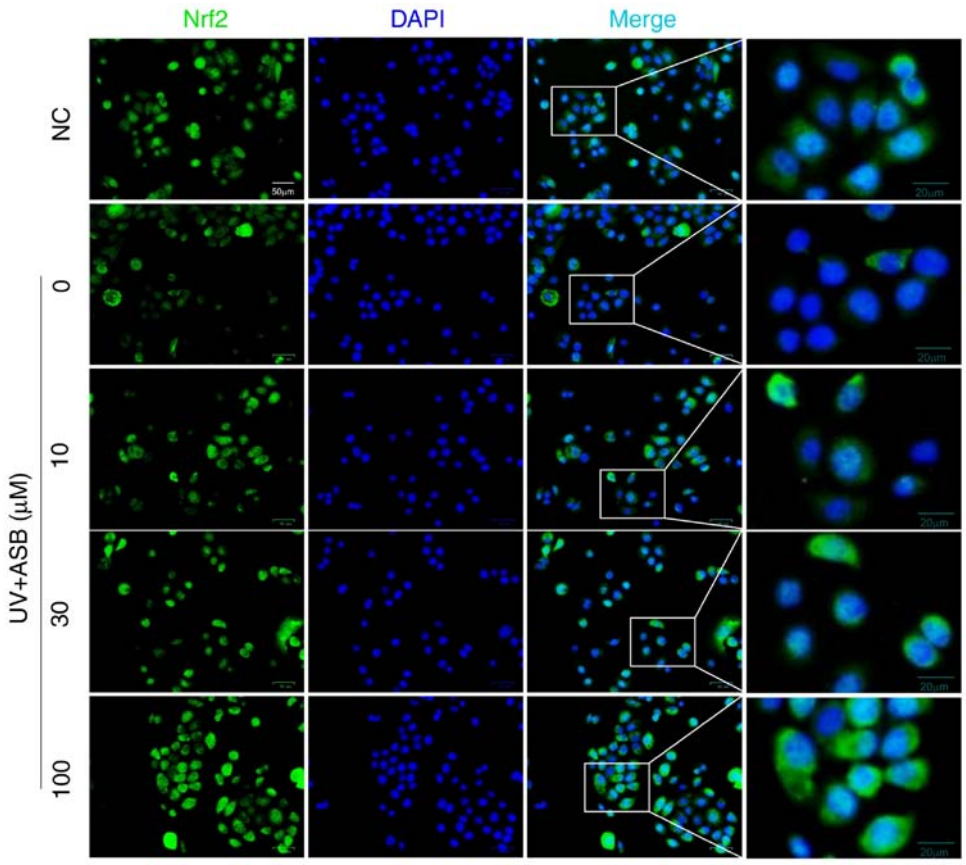

Figure 5. ASB increases the nuclear expression of Nrf2 in UV-induced HaCaT cells. The cells were preincubated with ASB (10, 30 and 100 μM) and irradiated with UV (90 mJ/cm^2). The fluorescence localization of Nrf2 was measured with immunofluorescence. An anti-Nrf2 antibody was used to detect Nrf2 localization (green) using a fluorescence microscope. DAPI staining indicated the locations of the nuclei (blue). ASB, andrographolide sodium bisulfite; UV, ultraviolet; Nrf2, nuclear factor E2-related factor 2; NC, normal control.

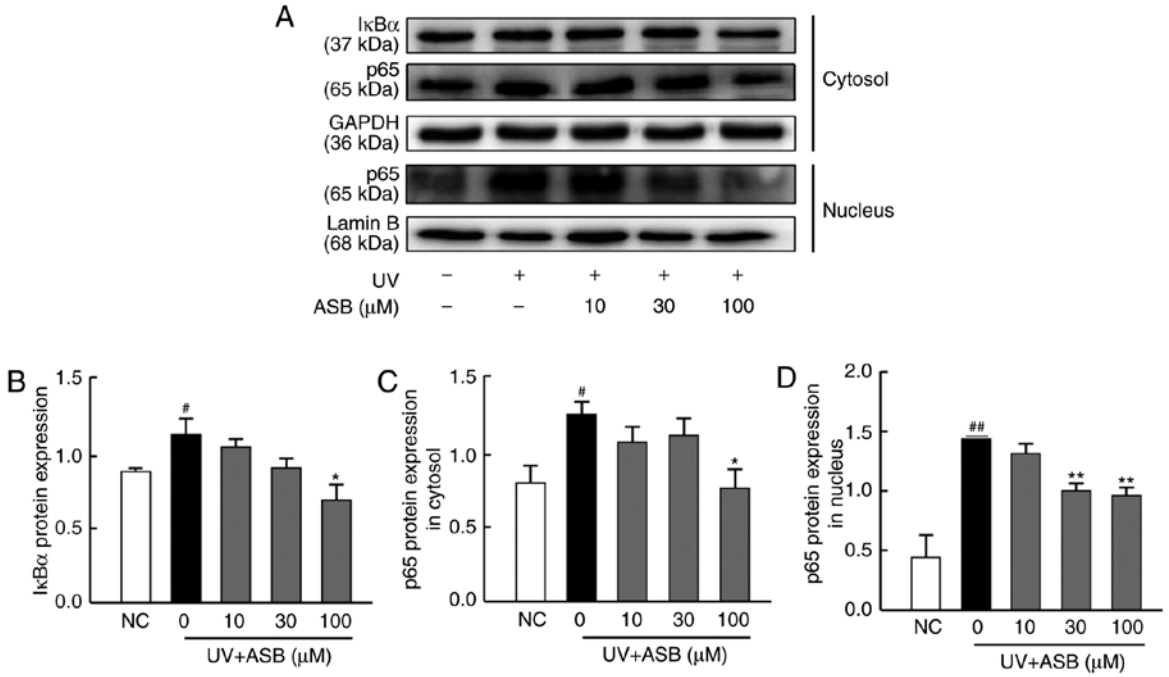

Figure 6. ASB inhibits the NF-κB signaling pathway in UV-induced HaCaT cells. The cells were preincubated with ASB (10, 30 and 100 μM) and irradiated by UV (90 mJ/cm^2). (A) Nuclear and cytoplasmic proteins were extracted; p65 and IκBα proteins were measured by western blotting. Relative changes in protein intensity were quantified for (B) IκBα, (C) cytosolic p65 and (D) nuclear p65 by densitometric analysis, and are presented as bar diagrams (n=3 for each group). $^{\#}$P<0.05, $^{\#\#}$P<0.01 vs. NC group; *P<0.05, **P<0.01 vs. UV-alone group. ASB, andrographolide sodium bisulfite; UV, ultraviolet; IκBα, NF-κB inhibitor-α; NC, normal control.

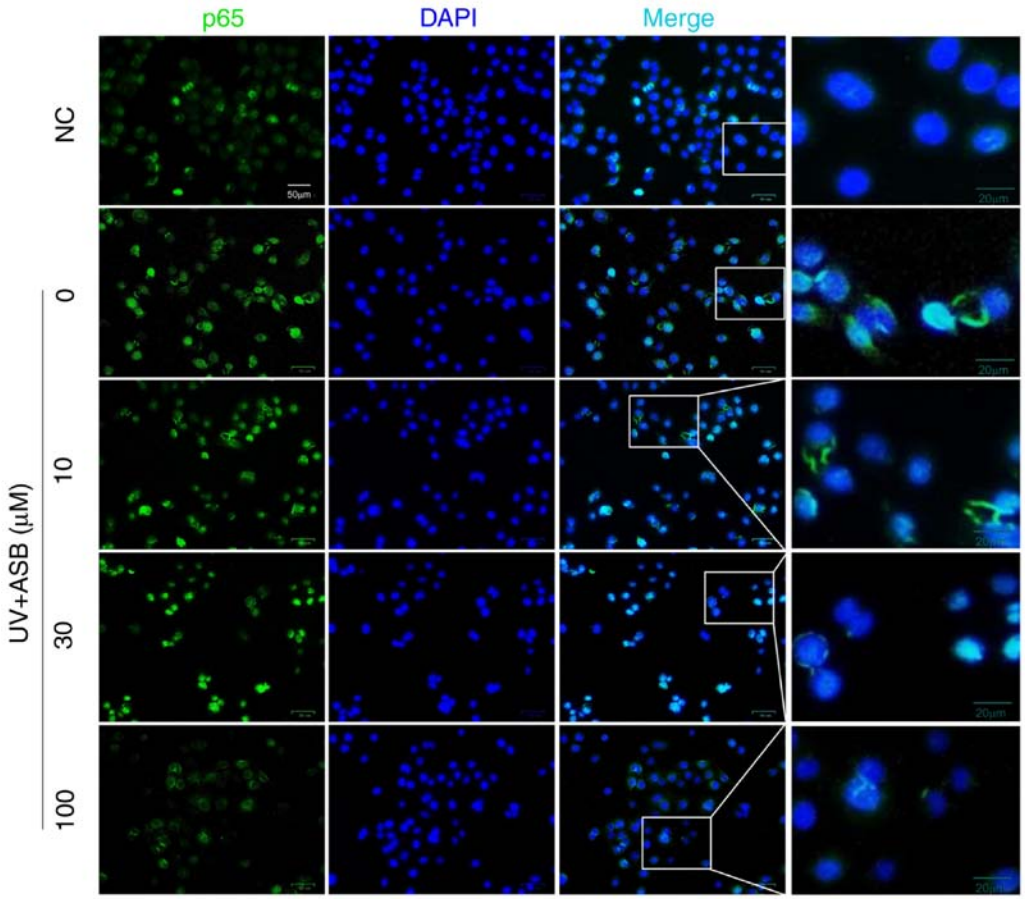

Figure 7. ASB decreases the nuclear expression of p65 in UV-induced HaCaT cells. The cells were preincubated with ASB (10, 30 and 100 μM) and irradiated by UV (90 mJ/cm^2). The fluorescence localization of p65 was measured with immunofluorescence. An anti-p65 antibody was used to detect p65 localization (green) using a fluorescence microscope. DAPI staining indicated the locations of nuclei (blue). ASB, andrographolide sodium bisulfite; UV, ultraviolet; NC, normal control.

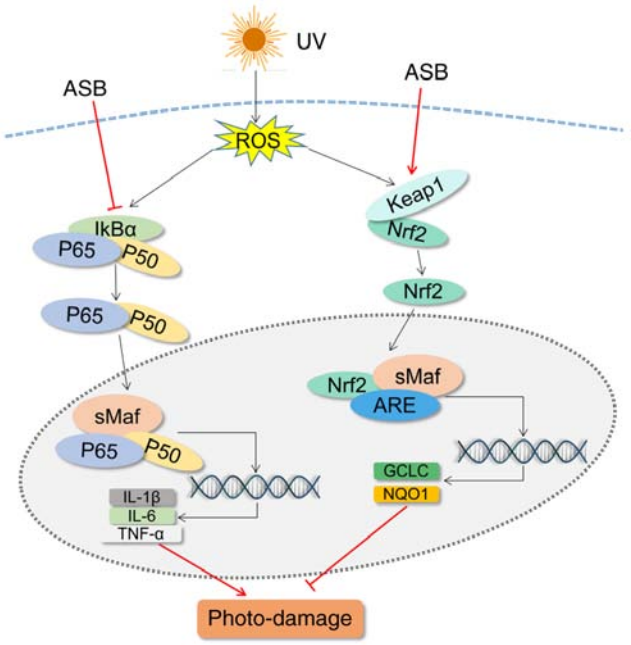

Figure 8. Schematic diagram of the mechanism of action of ASB in UV-induced photo-damage in HaCaT cells. UV, ultraviolet; ASB, andrographolide sodium bisulfite; ROS, reactive oxygen species; keap1, kelch-like ECH-associated protein 1; Nrf2, nuclear factor E2-related factor 2; IL, interleukin; TNF-α, tumor necrosis factor-α; GCLC, glutamate-cysteine ligase catalytic subunit; NQO1, NAD(P)H quinone oxidoreductase 1; IκBα, NF-κB inhibitor-α; ARE, antioxidant response element.

with Maf proteins and ARE, and subsequently regulates the expression of downstream antioxidant genes, such as GCLC and NQO1 (32). Nrf2 transcriptional activation and its antioxidant genes repair UV-induced skin inflammatory damage, protect cells against UV insult and decrease photo-oxidative damage (33). It has been demonstrated that andrographolide markedly suppresses oxidative stress injury by increasing Nrf2 activation and the expression levels of Nrf2 downstream genes, both *in vivo* and *in vitro* (34). In the present study, increased Nrf2 nuclear localization was observed after ASB treatment in HaCaT cells, which was followed by the upregulation of GCLC and NQO1 mRNA levels. These results indicated that ASB could activate Nrf2 signaling to suppress the UV-induced oxidative stress present in photo-damaged cells.

Recent studies have suggested that there is a potential dynamic balance system and possible crosstalk between the Nrf2 and NF-κB pathways (35,36). Liu *et al* (37) demonstrated that NF-κB competitively dissociates Nrf2 from CREB-binding protein and facilitates the recruitment of histone deacetylase 3 to MafK, resulting in the inactivation of Nrf2. Overexpression of p65 decreases Nrf2 protein levels by promoting Nrf2 ubiquitination (38). By contrast, inhibition of Nrf2 expression also accelerates the activation of NF-κB. For instance, the absence of Nrf2 enhances NF-κB-dependent inflammation following scratch injury (39). In addition, phenethyl isothiocyanate and sulforaphane, as Nrf2 activators, inhibit NF-κB subunit p65 nuclear translocation, consequently inactivating the NF-κB signaling pathway (40). In the present study, the timepoint results represented a new phenomenon, in that the protein expression levels of IκBα and cytoplasmic p65 were continuously increased, while the protein expression levels of Nrf2 pathway proteins were increased at first and then decreased, between 0 and 6 h after UV irradiation. This indicated the presence of a dynamic balance between the NF-κB and Nrf2 signaling pathways in HaCaT cells, and continuous UV stimulation rendered the negative regulation of Nrf2 by NF-κB advantageous. In addition, the present study indicated that the Nrf2 and NF-κB pathways share common effectors and regulatory points, and that they can be activated by ROS at the same time (41). Therefore, there is a likely to be a dynamic balance between the NF-κB and Nrf2 signaling pathways in HaCaT cells.

The present study revealed that ASB inhibited UV-ROS-induced inflammation and oxidative stress following skin cell damage by downregulating the NF-κB pathway and activating the Nrf2 pathway (Fig. 8). Thus, ASB may be considered to be a promising strategy for preventing skin photo-damage. In UV-induced photoaging models, biological functions and genetic variations are different between HaCaT cells and normal human keratinocytes, which may impact the cellular responses to UV irradiation. Thus, normal human keratinocytes should be used in future research.

Acknowledgements

Not applicable.

Funding

This study was supported by National Natural Science Foundation of China (grant no. 81503318), Guangzhou University of Chinese Medicine Young Talent Project (grant no. QNYC20170106), and Guangdong Public Welfare Research and Capacity Building Projects (grant no. 2016A020217016).

Availability of data and materials

All data generated or analyzed during this study are included in this published article.

Authors' contributions

ZRS and JYXZ made substantial contributions to the design of the work. BQL, YC and JY were involved in the study conception and design. MLW and QYZ performed the experiments, analyzed the data and wrote the paper. YHL and YFH were involved in the experiments in the present study. BQL contributed to drafting and revising the manuscript. All authors read and approved the manuscript.

Ethics approval and consent to participate

Not applicable.

Patient consent for publication

Not applicable.

Competing interests

The authors declare that they have no competing interests.

References

1. Battie C and Verschoore M: Cutaneous solar ultraviolet exposure and clinical aspects of photodamage. Indian J Dermatol Venereol Leprol 78 (Suppl 1): S9-S14, 2012.
2. Ogden S, Samuel M and Griffiths CE: A review of tazarotene in the treatment of photodamaged skin. Clin Interv Aging 3: 71-76, 2008.
3. Kageyama H and Waditee-Sirisattha R: Antioxidative, anti-inflammatory, and anti-aging properties of mycosporine-like amino acids: Molecular and cellular mechanisms in the protection of skin-aging. Mar Drugs 17: E222, 2019.
4. Puizina-Ivić N: Skin aging. Acta Dermatovenerol Alp Pannonica Adriat 17: 47-54, 2008.
5. Wu SL, Li H, Zhang XM and Li ZF: Optical features for chronological aging and photoaging skin by optical coherence tomography. Lasers Med Sci 28: 445-450, 2013.
6. Schuch AP, Moreno NC, Schuch NJ, Menck CFM and Garcia CCM: Sunlight damage to cellular DNA: Focus on oxidatively generated lesions. Free Radic Biol Med 107: 110-124, 2017.
7. Kim HK: Protective effect of garlic on cellular senescence in UVB-exposed HaCaT human keratinocytes. Nutrients 8: E464, 2016.
8. Zhang JX, Wang XL, Vikash V, Ye Q, Wu D, Liu Y and Dong W: ROS and ROS-mediated cellular signaling. Oxid Med Cell Longev 2016: 4350965, 2016.
9. Lee B, Moon KM, Son S, Yun HY, Han YK, Ha YM, Kim DH, Chung KW, Lee EK, An HJ, *et al*: (2R/S,4R)-2-(2,4-Dihydroxyphenyl)thiazolidine-4-carboxylic acid prevents UV-induced wrinkle formation through inhibiting NF-κB-mediated inflammation. J Dermatol Sci 79: 313-316, 2015.
10. Pires BRB, Silva RCMC, Ferreira GM and Abdelhay E: NF-kappaB: Two sides of the same coin. Genes (Basel) 9: E24, 2018.
11. Kim M, Park YG, Lee HJ, Lim SJ and Nho CW: Youngiasides A and C isolated from youngia denticulatum inhibit UVB-induced MMP expression and promote type I procollagen production via repression of MAPK/AP-1/NF-κB and activation of AMPK/Nrf2 in HaCaT cells and human dermal fibroblasts. J Agric Food Chem 63: 5428-5438, 2015.
12. Muzaffer U, Paul VI, Prasad NR, Karthikeyan R and Agilan B: Protective effect of *juglans regia* L. Against ultraviolet B radiation induced inflammatory responses in human epidermal keratinocytes. Phytomedicine 42: 100-111, 2018.
13. Kim S and Chung JH: Berberine prevents UV-induced MMP-1 and reduction of type I procollagen expression in human dermal fibroblasts. Phytomedicine 15: 749-753, 2008.
14. Thimmulappa RK, Lee H, Rangasamy T, Reddy SP, Yamamoto M, Kensler TW and Biswal S: Nrf2 is a critical regulator of the innate immune response and survival during experimental sepsis. J Clin Invest 116: 984-995, 2006.
15. Schäfer M and Werner S: Nrf2-A regulator of keratinocyte redox signaling. Free Radic Biol Med 88(Pt B): 243-252, 2015.
16. Zhang DD and Hannink M: Distinct cysteine residues in Keap1 are required for Keap1-dependent ubiquitination of Nrf2 and for stabilization of Nrf2 by chemopreventive agents and oxidative stress. Mol Cell Biol 23: 8137-8151, 2003.
17. Wang W, Guan C, Sun X, Zhao Z, Li J, Fu X, Qiu Y, Huang M, Jin J and Huang Z: Tanshinone IIA protects against acetaminophen-induced hepatotoxicity via activating the Nrf2 pathway. Phytomedicine 23: 589-596, 2016.
18. Hseu YC, Korivi M, Lin FY, Li ML, Lin RW, Wu JJ and Yang HL: Trans-cinnamic acid attenuates UVA-induced photoaging through inhibition of AP-1 activation and induction of Nrf2-mediated antioxidant genes in human skin fibroblasts. J Dermatol Sci 90: 123-134, 2018.
19. Saw CL, Huang MT, Liu Y, Khor TO, Conney AH and Kong AN: Impact of Nrf2 on UVB-induced skin inflammation/photoprotection and photoprotective effect of sulforaphane. Mol Carcinog 50: 479-486, 2011.
20. Guo W, Liu W, Chen G, Hong S, Qian C, Xie N, Yang X, Sun Y and Xu Q: Water-soluble andrographolide sulfonate exerts anti-sepsis action in mice through down-regulating p38 MAPK, STAT3 and NF-κB pathways. Int Immunopharmacol 14: 613-619, 2012.
21. Lu H, Zhang XY, Zhou YQ, Wen X and Zhu LY: Proteomic alterations in mouse kidney induced by andrographolide sodium bisulfite. Acta Pharmacol Sin 32: 888-894, 2011.
22. Lu H, Zhang XY, Wang YQ, Zheng XL, Yin-Zhao, Xing WM and Zhang Q: Andrographolide sodium bisulfate-induced apoptosis and autophagy in human proximal tubular endothelial cells is a ROS-mediated pathway. Environ Toxicol Pharmacol 37: 718-728, 2014.
23. Liang E, Liu X, Du Z, Yang R and Zhao Y: Andrographolide ameliorates diabetic cardiomyopathy in mice by blockage of oxidative damage and NF-κB-mediated inflammation. Oxid Med Cell Longev 2018: 9086747, 2018.
24. Zhan JYX, Wang XF, Liu YH, Zhang ZB, Wang L, Chen JN, Huang S, Zeng HF and Lai XP: Andrographolide sodium bisulfate prevents UV-induced skin photoaging through inhibiting oxidative stress and inflammation. Mediat Inflamm 2016: 3271451, 2016.
25. Sun S, Jiang P, Su W, Xiang Y, Li J, Zeng L and Yang S: Wild chrysanthemum extract prevents UVB radiation-induced acute cell death and photoaging. Cytotechnology 68: 229-240, 2016.
26. Li H, Gao A, Jiang N, Liu Q, Liang B, Li R, Zhang E, Li Z and Zhu H: Protective effect of curcumin against acute ultraviolet B irradiation-induced photo-damage. Photochem Photobiol 92: 808-815, 2016.
27. Gong M, Zhang P, Li C, Ma X and Yang D: Protective mechanism of adipose-derived stem cells in remodelling of the skin stem cell niche during photoaging. Cell Physiol Biochem 51: 2456-2471, 2018.
28. Cuadrado A, Martin-Moldes Z, Ye J and Lastres-Becker I: Transcription factors NRF2 and NF-κB are coordinated effectors of the Rho family, GTP-binding protein RAC1 during inflammation. J Biol Chem 289: 15244-15258, 2014.
29. Xian DH, Gao XQ, Xiong X, Xu J, Yang L, Pan L and Zhong J: Photoprotection against UV-induced damage by skin-derived precursors in hairless mice. J Photochem Photobiol B 175: 73-82, 2017.
30. Feng XX, Yu XT, Li WJ, Kong SZ, Liu YH, Zhang X, Xian YF, Zhang XJ, Su ZR and Lin ZX: Effects of topical application of patchouli alcohol on the UV-induced skin photoaging in mice. Eur J Pharm Sci 63: 113-123, 2014.
31. Pollet M, Shaik S, Mescher M, Frauenstein K, Tigges J, Braun SA, Sondenheimer K, Kaveh M, Bruhs A, Meller S, *et al*: The AHR represses nucleotide excision repair and apoptosis and contributes to UV-induced skin carcinogenesis. Cell Death Differ 25: 1823-1836, 2018.
32. Katsuoka F, Motohashi H, Ishii T, Aburatani H, Engel JD and Yamamoto M: Genetic evidence that small Maf proteins are essential for the activation of antioxidant response element-dependent genes. Mol Cell Biol 25: 8044-8051, 2005.
33. Jastrzab A, Gegotek A and Skrzydlewska E: Cannabidiol regulates the expression of keratinocyte proteins involved in the inflammation process through transcriptional regulation. Cells 8: E827, 2019.
34. Yan H, Huang Z, Bai Q, Sheng Y, Hao Z, Wang Z and Ji L: Natural product andrographolide alleviated APAP-induced liver fibrosis by activating Nrf2 antioxidant pathway. Toxicology 396-397: 1-12, 2018.
35. Herpers B, Wink S, Fredriksson L, Di Z, Hendriks G, Vrieling H, de Bont H and van de Water B: Activation of the Nrf2 response by intrinsic hepatotoxic drugs correlates with suppression of NF-κB activation and sensitizes toward TNFα-induced cytotoxicity. Arch Toxicol 90: 1163-1179, 2016.
36. Chiou YS, Huang QR, Ho CT, Wang YJ and Pan MH: Directly interact with Keap1 and LPS is involved in the anti-inflammatory mechanisms of (-)-epicatechin-3-gallate in LPS-induced macrophages and endotoxemia. Free Radic Biol Med 94: 1-16, 2016.
37. Liu GH, Qu J and Shen X: NF-kappaB/p65 antagonizes Nrf2-ARE pathway by depriving CBP from Nrf2 and facilitating recruitment of HDAC3 to MafK. Biochim Biophys Acta 1783: 713-727, 2008.
38. Yu M, Li H, Liu Q, Liu F, Tang L, Li C, Yuan Y, Zhan Y, Xu W, Li W, *et al*: Nuclear factor p65 interacts with Keap1 to repress the Nrf2-ARE pathway. Cell Signal 23: 883-892, 2011.
39. Pan H, Wang H, Wang X, Zhu L and Mao L: The absence of Nrf2 enhances NF-κB-dependent inflammation following scratch injury in mouse primary cultured astrocytes. Mediators Inflamm 2012: 217580, 2012.
40. Cheung KL and Kong AN: Molecular targets of dietary phenethyl isothiocyanate and sulforaphane for cancer chemoprevention. AAPS J 12: 87-97, 2010.
41. Buelna-Chontal M and Zazueta C: Redox activation of Nrf2 and NF-κB: A double end sword? Cell Signal 25: 2548-2557, 2013.